JOURNAL OF SOLID STATE CHEMISTRY 101, 161–172 (1992)

The Crystal Structure and Electronic Properties of $Ba_4Ru_3MO_{12}$ (M = Li, Na, Mg, Zn)

P. D. BATTLE,* S. H. KIM, AND A. V. POWELL

Inorganic Chemistry Laboratory, South Parks Road, Oxford, OX1 3QR, United Kingdom

Received January 31, 1992; accepted April 29, 1992

The crystal structures of two new hexagonal perovskites, 6H-$Ba_4Ru_3LiO_{12}$ and 8H-$Ba_4Ru_3NaO_{12}$, have been refined from neutron powder diffraction data. The former shows *cch* stacking of the pseudo-close-packed BaO_3 layers in space group $P6_3/mmc$, a = 5.7828(1) and c = 14.1917(4) Å. The structure contains Ru_2O_9 dimers linked together by vertex-sharing MO_6 octahedra, where M represents a disordered distribution of Ru and Li. $Ba_4Ru_3NaO_{12}$ has a *ccch* stacking sequence in space group $P6_3mc$, a = 5.8142(1) and c = 19.2643(4) Å. The structure contains Ru_2O_9 dimers linked by vertex-sharing $RuNaO_{11}$ groups. Magnetic susceptibility measurements suggest that both compounds are magnetically ordered at low temperatures. Electrical conductivity measurements show that both are semiconductors. The preparation and electronic properties of the mixed valence compounds $Ba_4Ru_3MgO_{12}$ and $Ba_4Ru_3ZnO_{12}$ are also discussed.

Introduction

Ruthenium compounds have played a central role in our study of the electronic properties of transition metal oxides and we have paid particular attention to materials containing the metal in the oxidation state Ru(V). The reason for this interest is that, unlike most cations readily derived from the elements of the second transition series, Ru(V) shows a localized magnetic moment in its oxides, which are consequently insulators, often undergoing a transition to an antiferromagnetic state at low temperatures (*1*). This behavior can be contrasted with that of Ru(IV) oxides which are often metallic, for example, RuO_2 and $SrRuO_3$. The Ru(V) compounds studied to date adopt either the 6H-hexagonal (*2*) or pseudo-cubic (*1*) perovskite structures, and the transition metal is therefore octahedrally coordinated with the outer electron configuration $4d^3 : t_{2g}^3 e_g^0$. The observed electronic properties might then be regarded as predictable because the high correlation energy associated with the half-filled t_{2g} shell is likely to lead to localized electron behavior. However, none of the pseudo-cubic compounds studied, for example, Ba_2LaRuO_6 (*1*), has more than 50% of the 6-coordinate (B) sites occupied by Ru(V), and it is possible that an increase in the concentration of Ru(V) might lead to a change in electronic properties. Our attempts to prepare the concentrated compound $ARuO_3$ (A is a monovalent cation) have been unsuccessful, but we have succeeded in preparing the intermediate compounds $Ba_4Ru_3M^+O_{12}$ (M = Na, Li), and in this paper we describe their crystal struc-

* To whom correspondence should be addressed.

0022-4596/92 $5.00

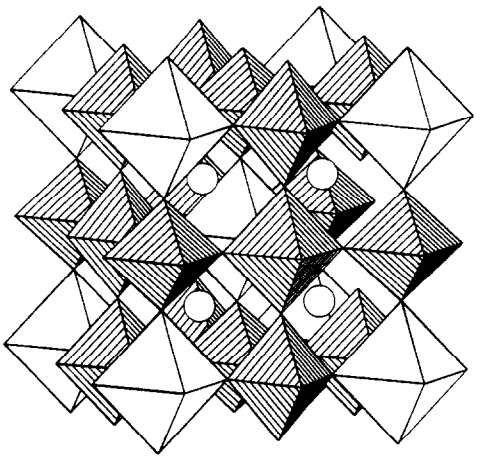

FIG. 1. The ordered cubic perovskite structure of $Ba_4Sb_3M^+O_{12}$ (M = Li, Na), showing a 3 : 1 ordered arrangement of Sb and M atoms. Open octahedra contain M atoms, and hatched octahedra contain Sb atoms. Ba atoms (circles) are in the voids formed by the octahedra.

tures, magnetic properties, and electrical conductivity. We have also prepared and characterized the mixed valence compounds $Ba_4Ru_3M^{2+}O_{12}$ (M = Mg, Zn). Our choice of target compound was initially determined by our previous observation (*3*) that there is a marked similarity between the structural chemistry of Ru(V) and that of Sb(V), coupled with an awareness of the preparation of the cubic perovskites $Ba_4Sb_3LiO_{12}$ and $Ba_4Sb_3NaO_{12}$ by Jacobson *et al.* (*4*) and Alonso *et al.* (*5*). Both of these materials have a body-centered cubic structure ($a \sim 8.2$ Å) with a 3 : 1 ordered arrangement of Sb(V) and M^+ over the octahedral sites, as drawn in Fig. 1; $Sr_4Sb_3NaO_{12}$ has subsequently been shown (*6*) to have a similar, albeit distorted, structure. We hoped to prepare isostructural Ru(V) analogues of these compounds, thus enabling us to study for the first time the electronic properties of an extended network of $Ru(V)O_6$ octahedra which are directly linked to one another by a common vertex. We shall show below that the new compounds do not have the anticipated crystal structure, but that they do nevertheless have interesting properties.

Experimental

Polycrystalline samples of $Ba_4Ru_3MO_{12}$ (M = Li, Mg, Na, Zn) were prepared from near stoichiometric mixtures of $BaCO_3$, MgO, ZnO, dried RuO_2 (Johnson Matthey "Specpure" reagents), Li_2CO_3, and Na_2CO_3 (BDH AnalaR reagents). In the case of $Ba_4Ru_3LiO_{12}$ and $Ba_4Ru_3NaO_{12}$, an excess (~10%) of alkali carbonates was used in order to offset their partial volatilization. The mixtures were ground, pelletized, and fired in alumina crucibles initially at 500°C overnight and then at 800°C (Li and Na) or 1100°C (Mg and Zn) for several days. The products were periodically quenched, reground, and characterized by X-ray powder diffraction using a Philips automated PW 1710 diffractometer operating with Cu$K\alpha$ radiation. The final X-ray powder diffraction patterns showed that all products were single-phase samples of hexagonal materials. $Ba_4Ru_3LiO_{12}$ and $Ba_4Ru_3NaO_{12}$ were dissolved in a mixture of HCl, HNO_3, and HF and analyzed for Li and Na by atomic absorption spectroscopy; the results were in good agreement with the values expected for ideal stoichiometry. We also attempted to make $Sr_4Ru_3M^+O_{12}$ (M = Na, Li) under the same conditions but X-ray diffraction patterns indicated that the products were multiphasic. Neutron diffraction data were collected on $Ba_4Ru_3LiO_{12}$ and $Ba_4Ru_3NaO_{12}$ at room temperature using the diffractometer D1a at ILL, Grenoble. The bank of 10 detectors was scanned through the angular range $0° \leq 2\theta \leq 156°$ in steps of 0.05°, the total data collection taking *ca.* 11 hr. Samples were contained in thin-walled vanadium cans of 16 mm diameter and the mean neutron wavelength was 1.9116 Å. Magnetic susceptibility measurements were performed in the temperature range 8 K $\leq T \leq$ 300 K using a Cryogenic S600C SQUID

magnetometer. Zero-field-cooled (zfc) and field-cooled (fc) measurements were made in applied fields of 5 (Li), 10 (Na), or 12 (Zn,Mg) kG. Electrical resistivity measurements were made between 77 and 300 K using a dc four-probe apparatus mounted in an Oxford Instruments CF 200 cryostat. Colloidal silver paint was used to make contacts on samples of dimensions 2 × 2 × 10 mm which had been cut from sintered pellets. The separation of the two inner (voltage) contacts was ~3 mm.

Results

Structural Characterization

Unit cell parameters for all the products were initially determined from the peak positions ($2\theta < 70°$) observed in the X-ray powder diffraction experiments. Profile analysis of the neutron diffraction data was carried out with the Brookhaven version of the Rietveld method (*7*, *8*) using a pseudo-Voigt peak shape function. The following coherent scattering lengths were used: b (Ba) = 0.520, b (Ru) = 0.730, b (Li) = −0.214, b (Na) = 0.360, b (O) = 0.581 × 10^{-12} cm (*9*). The background level was estimated by interpolation between regions of the profile where there were no Bragg peaks. The data were refined until all parameter shifts were less than 0.3 standard deviations.

(*i*) $Ba_4Ru_3NaO_{12}$. The X-ray diffraction pattern of $Ba_4Ru_3NaO_{12}$ could be indexed in a hexagonal unit cell, the size of which was consistent with the adoption of an 8H-hexagonal perovskite structure. $Ba_4Ta_3LiO_{12}$ has previously (*10*) been shown to adopt an 8H structure with a *ccch* stacking sequence of close-packed BaO_3 layers in space group $P6_3/mmc$. This symmetry results in the formation of both corner-sharing and face-sharing octahedral sites and hence in the presence of $LiTaO_9$ dimers which are linked together by Ta_2O_{11} units; the Li and Ta atoms are disordered in the dimers. However, attempts to refine the crystal structure of $Ba_4Ru_3NaO_{12}$ using this model were unsuccessful, thus revealing that the assumed symmetry was incorrect. We therefore lowered the space group symmetry of our model to noncentrosymmetric $P6_3mc$. In the absence of the center of symmetry it is possible to vary the cation distribution over the octahedral sites, and our subsequent refinements showed that in $Ba_4Ru_3NaO_{12}$ the face-sharing sites are occupied solely by Ru, forming Ru_2O_9 dimers, whereas the corner-sharing sites are occupied by an ordered 1 : 1 distribution of Ru and Na. This arrangement is illustrated in Fig. 2. Profile analysis of 139 Bragg reflections using a total of 28 variable parameters to describe this model resulted

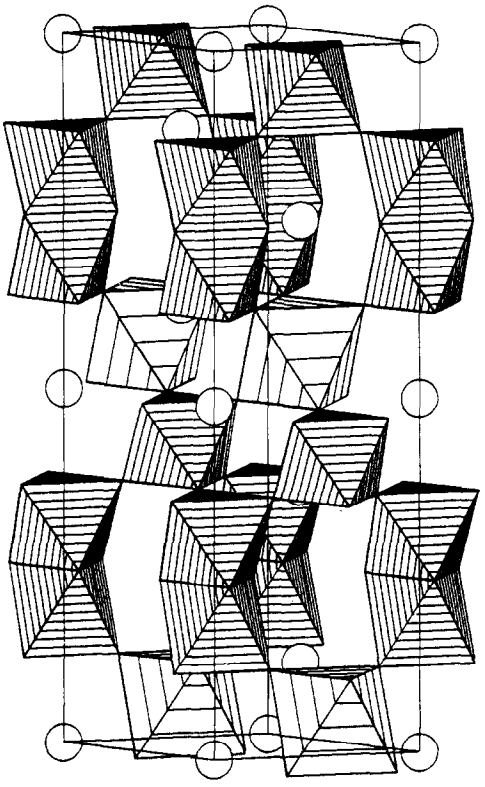

FIG. 2. The 8H-perovskite structure of $Ba_4Ru_3NaO_{12}$, showing a 1 : 1 ordered arrangement of Ru and Na atoms over the vertex-sharing octahedra. Lightly hatched octahedra contain Na atoms, and hatched octahedra contain Ru atoms. Circles are Ba atoms.

TABLE I

STRUCTURAL PARAMETERS FOR $Ba_4Ru_3NaO_{12}$ AT ROOM TEMPERATURE ($P6_3mc$)

Atom	Site	x	y	z	B_{iso} (Å^2)
Ba1	2*a*	0	0	0	0.62(3)
Ba2	2*b*	$\frac{1}{3}$	$\frac{2}{3}$	0.1229(5)	0.62(3)
Ba3	2*b*	$\frac{1}{3}$	$\frac{2}{3}$	0.3706(5)	0.62(3)
Ba4	2*b*	$\frac{1}{3}$	$\frac{2}{3}$	0.7465(5)	0.62(3)
Na	2*b*	$\frac{1}{3}$	$\frac{2}{3}$	0.5595(7)	0.63(5)
Ru1	2*b*	$\frac{1}{3}$	$\frac{2}{3}$	0.9366(5)	0.63(5)
Ru2	2*a*	0	0	0.3203(6)	0.71(4)
Ru3	2*a*	0	0	0.1824(5)	0.71(4)
O1	6*c*	0.4876(3)	0.5124(3)	−0.0097(5)	0.62(2)
O2	6*c*	0.8442(4)	0.1558(4)	0.1287(5)	0.62(2)
O3	6*c*	0.8345(4)	0.1656(4)	0.3725(5)	0.62(2)
O4	6*c*	0.8479(2)	0.1521(2)	0.7532(5)	0.62(2)

Note. a = 5.8142(1) Å, c = 19.2643(4) Å.

in the agreement indices R_{wpr} = 5.78% and R_I = 4.29%. The origin of the unit cell was defined by holding the coordinates of atom Ba1 constant. The unit cell parameters refined to the following values: a = 5.8142(1), c = 19.2643(4) Å. The final atomic coordinates and isotropic temperature factors are listed in Table I, and the corresponding bond lengths and angles in Table II; Ru2 and Ru3 lie within the face-sharing octahedra, with O4 in the common face. The final observed, calculated, and difference diffraction profiles are plotted in Fig. 3. The most obvious discrepancy is also apparent in the data collected on $Ba_4Ru_3LiO_{12}$ (see below) and that collected previously on $Ba_3CoRu_2O_9$ (*2*) and we therefore believe that it is likely to be instrumental in origin.

(*ii*) $Ba_4Ru_3LiO_{12}$. All the reflections in the X-ray diffraction pattern of $Ba_4Ru_3LiO_{12}$

TABLE II

BOND LENGTHS (Å) AND BOND ANGLES (°) IN $Ba_4Ru_3NaO_{12}$ AT ROOM TEMPERATURE

Ba1–O1	2.92(1) × 6	Ba2–O1	2.99(1) × 3	Ba3–O1	2.93(1) × 3	Ba4–O2	2.89(1) × 3
Ba1–O2	2.93(1) × 3	Ba2–O2	2.91(1) × 6	Ba3–O3	2.91(1) × 6	Ba4–O3	2.96(1) × 3
Ba1–O3	2.97(1) × 3			Ba3–O4	2.91(1) × 3	Ba4–O4	2.91(1) × 6
Na–O1	2.24(2) × 3	Ru1–O1	1.87(1) × 3	Ru2–O3	1.95(2) × 3	Ru3–O2	1.88(1) × 3
Na–O2	2.23(2) × 3	Ru1–O3	2.09(1) × 3	Ru2–O4	2.01(2) × 3	Ru3–O4	2.05(1) × 3
Ru2–Ru3	2.66(2)						
O1–O1	2.69(1) × 2	O2–O2	2.72(1) × 2	O3–O3	2.89(1) × 2	O4–O4	2.65(1) × 2
O1–O3	2.79(1) × 2	O2–O4	2.86(1) × 2	O3–O3′	2.93(1) × 2		
				O3–O4	2.80(1) × 2		
O1–Na–O1	88.3	O1–Ru1–O1	92.3	O3–Ru2–O3	95.7		
O1–Na–O2	179.7	O3–Ru1–O1	177.5	O3–Ru2–O4	90.4		
O2–Na–O2	87.9	O3–Ru1–O3	88.7	O4–Ru2–O4	82.8		
O2–Ru3–O2	92.6	Ru2–O3–Ru1	174.9				
O2–Ru3–O4	93.1	Ru1–O1–Na	177.2				
O4–Ru3–O4	80.6	Na–O2–Ru3	176.6				

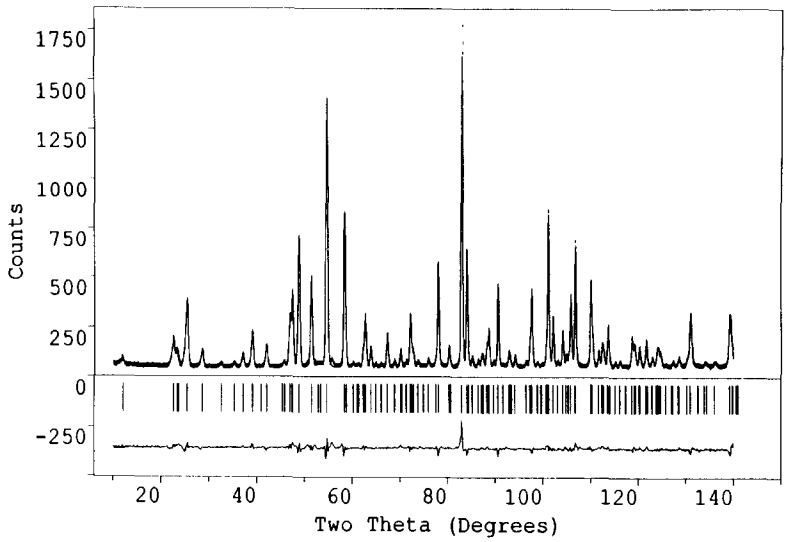

FIG. 3. The observed (···), calculated (—), and difference neutron diffraction profiles of $Ba_4Ru_3NaO_{12}$ at room temperature. Reflection positions are marked.

could be indexed in a hexagonal unit cell, the size of which was consistent with the adoption of a 6H-hexagonal perovskite structure. The neutron diffraction data were refined in space group $P6_3/mmc$ with a *cch* stacking sequence for the close-packed BaO_3 layers. In this rather common structure, the 6-coordinate cations lie either in an M_2O_9 dimer or in a single corner-sharing octahedron that links different dimers together. Refinement of the 20 parameters needed to describe this model, using the intensities of 103 Bragg reflections, led to the agreement indices R_{wpr} = 5.51%, R_I = 2.43%. The refined structural parameters are listed in Table III and the bond lengths and bond angles are given in Table IV. The Ru and Li occupation numbers are also given in Table III. The face-sharing octahedra are predominantly occupied by Ru^{5+} ions, but a small concentration of Li^+ ions is also present (Ru1/Li1, with O1 in the common face). The remaining Ru and Li cations are disordered over the vertex-sharing octahedra (Ru2/Li2, linked through O2). No evidence was found for partial occupancy of the oxygen sites. The structure is drawn in Fig. 4, and the final diffraction profiles appear in Fig. 5.

(*iii*) $Ba_4Ru_3M^{2+}O_{12}$ (M = *Mg, Zn*). As in the case of $Ba_4Ru_3LiO_{12}$, the X-ray powder diffraction patterns of $Ba_4Ru_3MgO_{12}$ and $Ba_4Ru_3ZnO_{12}$ indicated that both compounds adopt the 6H-perovskite structure. A comparison of the observed X-ray data with simulations produced using the computer program LAZY-PULVERIX (*11*) suggested that all the face-sharing octahedra are occupied by Ru and that the M^{2+} ions and the remainder of the Ru ions are disordered over the vertex-sharing octahedra. The unit cell parameters of $Ba_4Ru_3ZnO_{12}$ (a = 5.7585(7), c = 14.128(2) Å) are larger than those of the Mg compound (a = 5.7511(5), c = 14.112(1) Å, in agreement with expectations based on the difference in the octahedral ionic radii of M^{2+} (*12*).

Magnetic Measurements

The molar magnetic susceptibility of $Ba_4Ru_3LiO_{12}$ is plotted as a function of tem-

TABLE III

STRUCTURAL PARAMETERS FOR $Ba_4Ru_3LiO_{12}$ AT ROOM TEMPERATURE ($P6_3/mmc$)

Atom	Site	x	y	z	B_{iso} (Å^2)	N^a
Ba1	$2b$	0	0	$\frac{1}{4}$	0.82(5)	
Ba2	$4f$	$\frac{1}{3}$	$\frac{2}{3}$	0.9110(2)	0.56(4)	
Ru1	$4f$	$\frac{1}{3}$	$\frac{2}{3}$	0.1549(1)	0.70(3)	0.975(2)
Li1	$4f$	$\frac{1}{3}$	$\frac{2}{3}$	0.1549(1)	0.70(3)	0.025(2)
Ru2	$2a$	0	0	0	0.70(3)	0.299(2)
Li2	$2a$	0	0	0	0.70(3)	0.701(2)
O1	$6h$	0.4855(2)	−0.0289(4)	$\frac{1}{4}$	0.75(3)	
O2	$12k$	0.1722(1)	0.3445(3)	0.4163(1)	1.03(2)	

Note. a = 5.7828(1) Å, c = 14.1917(4) Å.
[a] N is the fractional site occupancy.

perature in Fig. 6. At temperatures above ~200K the zfc and fc susceptibilities are equal and increase slightly with temperature, but at lower temperatures they diverge. The zfc curve shows local maxima at 100 and 40 K and the fc curve has inflections at the same temperatures. In the case of $Ba_4Ru_3NaO_{12}$ the divergence of the zfc and fc data is apparent below 270 K, with maxima occuring at 260 and 110 K, as shown in Fig. 7. The temperature dependence of the molar magnetic susceptibilities of $Ba_4Ru_3MgO_{12}$ and $Ba_4Ru_3ZnO_{12}$ is shown in Fig. 8. In the high temperature region ($T > 70$ K), χ_m rises steadily with an increase in temperature, whereas at low temperature ($T < 70$ K) a minimum is observed and the fc curve diverges from the zfc data. The complex magnetic behavior of all these compounds will be discussed below in terms of the competition between the different magnetic interactions present.

Electrical Measurements

The results of the electrical resistivity measurements are shown in Fig. 9. $Ba_4Ru_3ZnO_{12}$ was not included in this experiment. All the samples are semiconductors in the temperature range 77–300 K. Attempts to fit the data to a simple Arrhenius model were unsuccessful, as were those based on a small-polaron mechanism. However, excellent agreement was obtained in the case of $Ba_4Ru_3MgO_{12}$ when the experimental data were fitted to the expression

$$\rho = \rho_0(T/T_0)^{1/2}\exp((T_0/T)^{\nu})$$

with $\nu = \frac{1}{2}$, consistent with the conductivity

TABLE IV

BOND LENGTHS (Å) AND BOND ANGLES (°) IN $Ba_4Ru_3LiO_{12}$ AT ROOM TEMPERATURE

Ba1–O1	2.895(3) × 6	Ba2–O1	2.918(4) × 3	Ru/Li1–O1	2.036(3) × 3
Ba1–O2	2.924(2) × 6	Ba2–O2	2.893(4) × 6	Ru/Li1–O2	1.904(3) × 3
		Ba2–O2′	2.934(4) × 3	Ru/Li2–O2	2.094(2) × 6
Ru/Li1–Ru/Li2	2.700(1)		O1–O1	2.640(4) × 2	
			O1–O2	2.836(3) × 4	
Ru/Li2–O2–Ru/Li1	177.5		O2–Ru/Li2–O2	89.0	
O1–Ru/Li1–O1	80.8	O2–Ru/Li1–O1	92.0	O1–Ru/Li1–O2	170.5

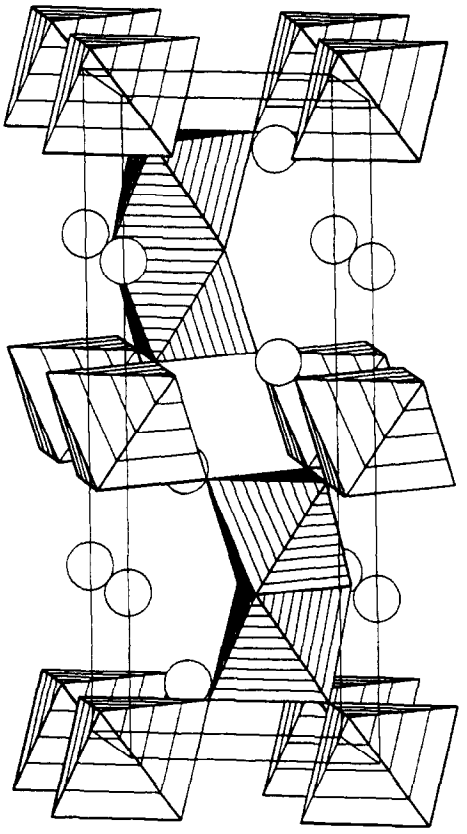

FIG. 4. The 6H-perovskite structure of $Ba_4Ru_3LiO_{12}$. The face-sharing octahedra are predominantly occupied by Ru atoms. The remaining Ru and Li atoms are disordered over the vertex-sharing octahedra. Circles are Ba atoms.

behavior predicted by Efros and Shklovskii (*13*) for compounds in which a Coulomb interaction between localized electrons creates an energy gap near the Fermi level. The data on $Ba_4Ru_3NaO_{12}$ and $Ba_4Ru_3LiO_{12}$ could also be fitted using the above equation. The values of ν were badly defined in these cases (~0.3) but they suggested that a variable range hopping (VRH) mechanism might be operating (*14*). The determination of the exponent ν is difficult owing to the limited temperature range over which measurements were performed. Furthermore, conductivity measurements made on polycrystalline samples, albeit sintered, will contain a contribution from the conductivity of grain boundaries. We were unable to make the thermopower measurements that would have enabled us to eliminate this effect, and the validity of the various models cannot therefore be considered proven.

Discussion

$Ba_4Ru_3NaO_{12}$ and $Ba_4Ru_3LiO_{12}$ are hexagonal perovskites rather than the cubic, or pseudo-cubic, compounds that we had hoped to prepare. The energy balance between these two structures can be very delicate, depending on relative cation size (r_B/r_A), the Madelung energy, the character of the B–O bonds, and the possibility of B–B bonding (*15*), and it is interesting to consider how these different factors influence the crystal structures of the compounds under discussion. The cubic perovskite structure ideally requires $(r_A + r_O) = \sqrt{2}(r_B + r_O)$, and a ratio r_B/r_A much in excess of this ideal leads to the introduction of hexagonal stacking among the close-packed AO_3 layers. This allows the introduction of relatively large cations on the A site, but it also introduces strong electrostatic repulsions between pairs of B cations occupying octahedral sites which are linked by a common face. Ba_2LuRuO_6 (*16*) is a cubic perovskite with an average B–O distance of 2.065 Å; the corresponding distances in $Ba_4Ru_3NaO_{12}$ and $Ba_4Ru_3LiO_{12}$ are 2.04 and 2.03 Å, respectively. These data suggest that the former is slightly closer to the critical value of r_A/r_B that would have permitted the stabilization of a cubic phase, and this conclusion is further supported by the formation of an 8H structure which retains a relatively high proportion of cubic stacking among the AO_3 layers. The Li compound is more clearly in the hexagonal regime and consequently adopts a 6H structure with a lower proportion of cubic stacking. This explanation is not inconsistent with the adoption of a cubic

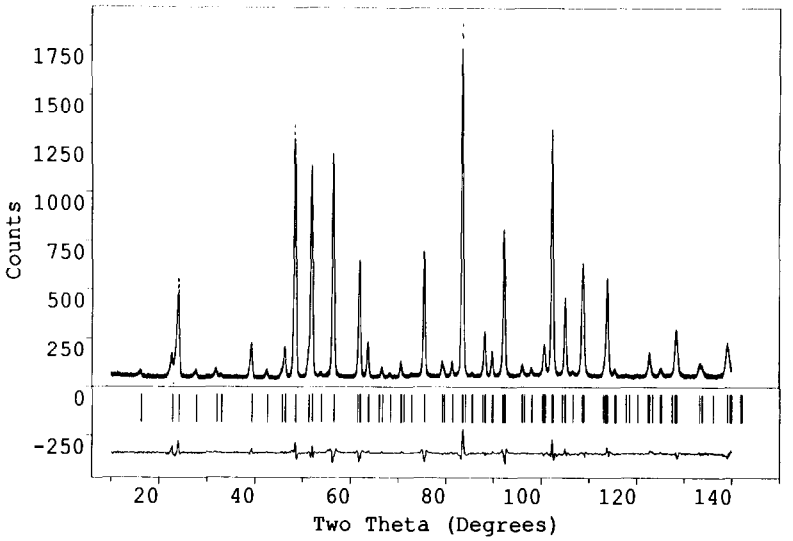

FIG. 5. The observed (···), calculated (—), and difference neutron diffraction profiles of $Ba_4Ru_3LiO_{12}$ at room temperature. Reflection positions are marked.

structure by $Ba_4LiSb_3O_{12}$, where the mean B–O distance is 2.056 Å, but in view of the formation of $Sr_4NaSb_3O_{12}$ (mean B–O = 2.05 Å) it is perhaps surprising that we were unable to make $Sr_4Ru_3NaO_{12}$. The presence of the smaller Sr^{2+} ion causes a reduction in the size of the octahedral sites available to Na^+ and Sb(V) and, even though the mean Na–O distance of 2.17 Å in $Sr_4NaSb_3O_{12}$ is somewhat shorter than that observed in $Ba_4Ru_3NaO_{12}$ (2.23 Å), the Sb(V) cations have to adopt an irregular coordination geometry in order to accommodate the Na^+ ions. It may be that the necessary distortion of the environment is energetically unfavorable in the case of the less-polarizable Ru(V) : $4d^3$ ions and that $Sr_4Ru_3NaO_{12}$ therefore cannot be prepared. The above discussion is based on considerations of cation size. Having used these criteria to account

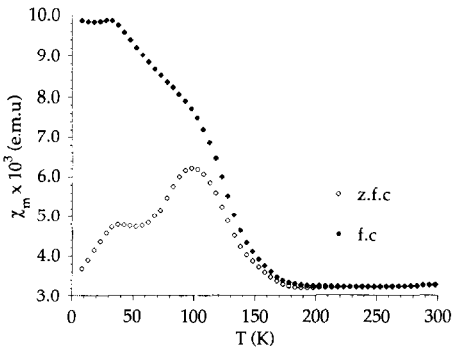

FIG. 6. The molar magnetic susceptibility of polycrystalline $Ba_4Ru_3LiO_{12}$ as a function of temperature.

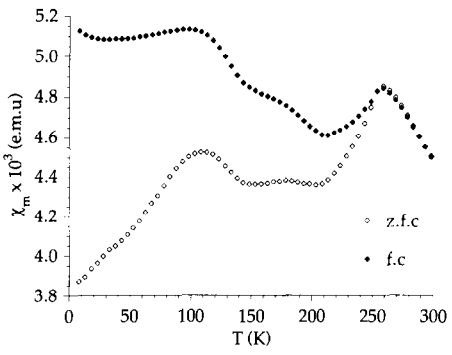

FIG. 7. The molar magnetic susceptibility of polycrystalline $Ba_4Ru_3NaO_{12}$ as a function of temperature.

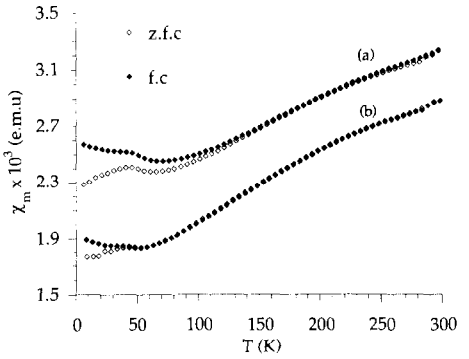

FIG. 8. The molar magnetic susceptibility of polycrystalline $Ba_4Ru_3M^{2+}O_{12}$ (M = (a) Mg, (b) Zn) as a function of temperature.

for the adoption of hexagonal structures, we must now identify the factors which dictate the observed distribution of cations over the 6-coordinate sites. The 8H-perovskite structure is not common in metal oxide chemistry, but in $Ba_4LiTa_3O_{12}$ and $Ba_4LiNb_3O_{12}$ (*10, 17*) the alkali-metal cation occupies a face-sharing octahedral site, and the corner-linked M_2O_{11} units contain only the pentavalent cation, in marked contrast to $Ba_4Ru_3NaO_{12}$ which contains Ru_2O_9 dimers linked together by $NaRuO_{11}$ units. The occupation of a face-sharing site by Li^+ in the former compounds reduces the electrostatic repulsion that would occur between two pentavalent cations in an M_2O_9 dimer. However, there are at least two important differences between the Li/Nb/Ta and Na/Ru compounds; first the $4d^3$ electron configuration of Ru(V) permits the formation of a Ru–Ru bond within the dimer, a source of stabilization that is not available to d^0 Nb(V) and Ta(V) cations, and second the size of Na^+ would introduce an excessive strain into the structure if the monovalent cation was to occupy a site within the dimers. As a consequence of these factors Ru_2O_9 dimers are formed, with the oxygen atoms in the common face of the octahedra (O4) moving toward one another in order to screen the electrostatic repulsion between the pentavalent cations, which are closer together in $Ba_4Ru_3NaO_{12}$ than in other compounds containing the same structural unit (*2*). The ordering of the Na^+ and Ru(V) cations in the $NaRuO_{11}$ units is easily understood in terms of the difference in size and charge between the two types of cation. Lattice energy and site potential calculations, carried out using an Ewald summation within the program GULP developed by Gale (*18*), are consistent with the results of our diffraction experiments, as can be seen from the data in Table V.

The cation ordering found in 6H-$Ba_4Ru_3LiO_{12}$ is incomplete, with the relatively small Li^+ cation occupying sites in both face-sharing and corner-sharing octahedra. However, the majority of the alkali metal cations occupy the latter sites, and this compound thus contains a significant number of Ru_2O_9 dimers. This result suggests that once again the formation of a Ru–Ru bond provides the stabilization necessary to compensate for the unfavorable electrostatic interaction.

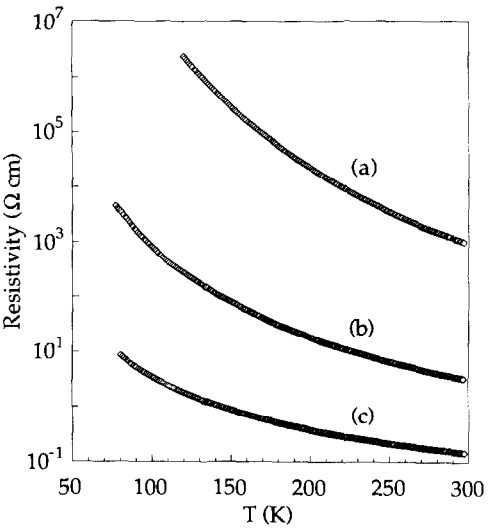

FIG. 9. The resistivity of polycrystalline $Ba_4Ru_3MO_{12}$ (M = (a) Na, (b) Li, (c) Mg) as a function of temperature.

TABLE V
SITE POTENTIALS IN $Ba_4Ru_3NaO_{12}$

Site	Potential (eV)
Ba1	−21.21
Ba2	−21.95
Ba3	−16.19
Ba4	−16.37
Na	−24.16
Ru1	−52.11
Ru2	−44.86
Ru3	−50.09
O1	19.06
O2	19.15
O3	29.63
O4	28.63

The magnetic data can be interpreted in the light of the refined crystal structures. It has been shown previously (*19*) that the superexchange between Ru(V) cations in an Ru_2O_9 dimer is strong enough to produce a susceptibility maximum in 6H-$Ba_3CaRu_2O_9$ at a temperature of ~450 K. The magnitude and temperature dependence of the magnetic susceptibility of $Ba_4Ru_3LiO_{12}$ in the temperature range 200 K $< T <$ 300 K leads us to suggest that extensive spin-pairing also occurs above room temperature within the dimers in this compound. However, $Ba_4Ru_3LiO_{12}$, unlike $Ba_3CaRu_2O_9$, also has a significant concentration (~30%) of magnetic cations in the corner-sharing octahedra. The exchange constant for coupling between corner-sharing and face-sharing sites is lower than that for coupling between pairs of face-sharing sites and these magnetic cations are likely to be paramagnetic at 300 K. However, they may well be responsible for the unusual behavior of the susceptibility which is observed below 200 K. The divergence of the zfc and fc data indicates that either a weak ferromagnetism or magnetic clusters with an uncompensated magnetic moment are present. This can be understood if we recognize that any particular Ru_2O_9 dimer will share corners with a statistical distribution of LiO_6 and RuO_6 octahedra. The observed susceptibility is a summation over all the possible combinations, and at temperatures low enough for antiferromagnetic coupling between face-sharing and corner-sharing sites to become significant it will undoubtedly include a contribution from extended clusters containing an odd number of Ru(V) cations which will therefore carry an uncompensated magnetic moment. The presence of magnetic cations on the corner-sharing sites provides a mechanism for magnetic coupling between dimers and as the temperature is lowered we would expect local magnetic coupling to develop into long-range antiferromagnetic order. Similar arguments have been used to account for the behavior of other disordered, magnetically diluted systems (*20*), although in this case the problem is made more complex by the presence of two distinct exchange interactions and the fact that in $Ba_4Ru_3LiO_{12}$ a small fraction of the dimers actually have the composition $RuLiO_9$ rather than Ru_2O_9, a point that we have not considered in the above discussion. It would be interesting to carry out low temperature neutron diffraction experiments in order to establish whether there is a transition to a phase showing long-range antiferromagnetic order in this compound and at what temperature it occurs. Such a transition does not occur in $Ba_3CaRu_2O_9$ (*21*), where the Ru_2O_9 dimers are magnetically isolated and the magnetic susceptibility has a less complex temperature dependence; it occurs at ~100K in the magnetically concentrated compound $Ba_3CoRu_2O_9$ (*22*). The situation in 8H-$Ba_4Ru_3NaO_{12}$ is slightly less complex because there is no significant level of disorder in the crystal structure. The strongest magnetic interaction will be that between pairs of Ru(V) cations in Ru_2O_9 dimers. The dimers are linked together, at one extreme only, by corner-sharing with RuO_6 octahedra, and the interaction between cations in

face-sharing and corner-sharing sites will be the second strongest. As can be seen from Fig. 2, the structure can be thought of as magnetic layers (2 + 1) octahedra thick, separated from each other by layers of corner-sharing NaO_6 octahedra. The interlayer interaction, going via the NaO_6 octahedra, will be the weakest of the superexchange couplings. It is likely that the Ru(V) cations within the dimers will be spin-paired below ~450 K and that the magnetic transition apparent at ~250 K in Fig. 7 occurs when the superexchange between face-sharing and corner-sharing sites becomes significant. The transition at ~100 K can then be interpreted as the onset of long-range antiferromagnetism, involving superexchange through the NaO_6 octahedra. Alternatively, long-range magnetic order might occur below 250 K with a spin reorientation occuring at ~100 K; the relative sharpness of the maximum at 250 K makes this an attractive model, although it would be an unusually high Neel temperature given that the superexchange interaction must pass through a diamagnetic layer of ~2.5 Å thickness. Low temperature neutron diffraction data are needed in order to test these hypotheses and to elucidate the difference between the zfc and fc susceptibilities. The low magnitudes of the magnetic susceptibilities shown in Fig. 8 for the mixed-valence compounds $Ba_4Ru_3MgO_{12}$ and $Ba_4Ru_3ZnO_{12}$ suggest that spin-pairing also occurs in these compounds. However, unlike the cases discussed above, no local susceptibility maximum is apparent in the temperature range covered by our experiment, although the zfc and fc susceptibilities do diverge at low temperatures, thus suggesting that the samples have a weak magnetisation below ~100 K (Mg) and 40 K (Zn). Again, neutron scattering experiments are needed before a detailed interpretation of these data can be made.

The electrical resistivity data plotted in Fig. 9 show an interesting trend. All three compounds are semiconductors, but with room temperature conductivities that span five orders of magnitude. The relatively high conductivity of 6H-$Ba_4Ru_3MgO_{12}$ is consistent with the Ru(IV)/Ru(V) mixed-valence formulation and can be explained by assuming that the extra electron in the 4*d* band (compared to $Ba_4Ru_3M^+O_{12}$) is only weakly localized. The conductivity of $Ba_4Ru_3LiO_{12}$ is significantly lower than that of $Ba_4Ru_3MgO_{12}$ because the concentration of mobile charge carriers is much lower when only Ru(V) is present. 8H-$Ba_4Ru_3NaO_{12}$ has a lower conductivity because there is a low concentration of charge carriers and the transition metal cations lie in two-dimensional blocks separated by layers of NaO_6 octahedra, as described in our discussion of the magnetic properties; in 6H-$Ba_4Ru_3LiO_{12}$ the transition metal is present, to some extent, on both 6-coordinate sites and the structure is essentially three dimensional. Clearly more work needs to be done before the electronic properties of these inadvertently prepared phases are fully understood.

Acknowledgments

We are grateful to SERC and ICI for funding A.V.P. and S.H.K., respectively. Dr. J. K. Cockcroft provided experimental assistance at ILL, and Dr. J. Gale advised us on the use of his program for the calculation of site potentials in $Ba_4Ru_3NaO_{12}$.

References

1. P. D. Battle, J. B. Goodenough, and R. Price, *J. Solid State Chem.* **46,** 234 (1983).
2. P. Lightfoot and P. D. Battle, *J. Solid State Chem.* **89,** 174 (1990).
3. P. Lightfoot and P. D. Battle, *Mater. Res. Bull.* **25,** 89 (1990).
4. A. J. Jacobson, B. M. Collins, and B. E. F. Fender, *Acta Crystallogr. B* **30,** 1705 (1974).
5. J. A. Alonso, E. Mzayek, and I. Rasines, *Mater. Res. Bull.* **22,** 69 (1987).
6. J. A. Alonso, E. Mzayek, and I. Rasines, *J. Solid State Chem.* **84,** 16 (1990).
7. H. M. Rietveld, *J. Appl. Crystallogr.* **2,** 65 (1969).
8. B. Toby, D. E. Cox, and P. Zolliker, unpublished work.

9. G. E. BACON, "Neutron Diffraction," 3rd ed., Oxford Univ. Press (Clarendon), Oxford (1975).
10. B. M. COLLINS, A. J. JACOBSON, AND B. E. F. FENDER, *J. Solid State Chem.* **10,** 29 (1974).
11. R. YVON, W. JEITSCHKO, AND E. PARTHE, *J. Appl. Crystallogr.* **10,** 73 (1977).
12. R. D. SHANNON, *Acta Crystallogr. A* **32,** 751 (1976).
13. A. L. EFROS AND B. I. SHKLOVSKII, *J. Phys. C Solid State Phys.* **8,** L49 (1975).
14. N. F. MOTT AND E. A. DAVIS, "Electronic Processes in Non-Crystalline Materials," Oxford Univ. Press (Clarendon), Oxford (1979).
15. J. B. GOODENOUGH AND J. A. KAFALAS, *J. Solid State Chem.* **6,** 493 (1973).
16. P. D. BATTLE AND C. W. JONES, *J. Solid State Chem.* **78,** 108 (1989).
17. T. NEGAS, R. S. ROTH, H. S. PARKER AND W. S. BROWER, *J. Solid State Chem.* **8,** 1 (1973).
18. J. GALE, General Utility Lattice Program, Royal Institution, London.
19. J. DARRIET, M. DRILLON, G. VILLENEUVE, AND P. HAGENMULLER, *J. Solid State Chem.* **19,** 213, (1976).
20. M. CYROT, *Solid State Commun.* **39,** 1009, (1981).
21. J. DARRIET, J. L. SOUBEYROUX, AND A. P. MURANI, *J. Phys. Chem. Solids,* **44,** 269 (1983).
22. P. D. BATTLE AND S. H. KIM, unpublished results.